RSC Advances

ROYAL SOCIETY OF CHEMISTRY

www.rsc.org/advances

The influence of hierarchical TiO_2 microspheres on the trap states distribution and charge transport/recombination dynamics in quantum dot sensitized solar cells

Xiao-Juan Shi, [a] Yi Wang, [a] Dapeng Wu, [b,c] Yujun Qin, [a] Xi-Cheng Ai, [a,*] Dongsheng Xu, [b] and Jian-Ping Zhang [a]

[a]*Department of Chemistry, Renmin University of China, Beijing 100872, P.R. China.*

[b]*Colleage of Chemistry and Molecular Engineering, Peking University, Beijing 100871, P.R. China.*

[c]*School of Chemistry and Chemical Engineering, Henan Normal University, Henan Xinxiang 453007, P.R. China.*

*To whom correspondence should be addressed

Tel: +86-10-62516604; Fax: +86-10-62516444

E-mail: xcai@ruc.edu.cn (X.-C. Ai)

Abstract

Two different kinds of quantum dot sensitized solar cells (QDSSCs) were fabricated based on the photoanode materials P25 (Cell-P25) and hierarchical TiO_2 microspheres (HMS, Cell-HMS), respectively. The trap state distribution and charge transport/recombination dynamics are comparatively investigated by means of time-resolved charge extraction and transient photovoltage. The dynamics results prove that, compared to Cell-P25, Cell-HMS possesses higher density and lower characteristic energy of trap state, as well as 30% lower charge transport rate. In addition, the boundary level dividing lower-voltage iso-energetic charge recombination and higher-voltage multiple-trap limited charge recombination is experimentally determined. Furthermore, Cell-HMS is found to exhibit a slightly higher boundary voltage and a 96% lower recombination rate with respect to Cell-P25. A physical model is proposed to describe the influence of trap state distribution on charge transport/recombination, highlighting the importance of photoanode morphology in optimizing the photovoltaic performance of QDSSCs.

Keywords: Hierarchical TiO_2 microspheres, trap states, charge transport, charge recombination, quantum dot sensitized solar cells

1. Introduction

Since Nozik team replaced the organic dye in dye sensitized solar cells (DSSCs) with InP quantum dot (QD) and fabricated the first quantum dot sensitized solar cells (QDSSCs) in 1988,[1] such novel photovoltaic devices have attracted significant attention as the promising third-generation solar cell owing to the high energy conversion efficiency and low cost.[2-4] In QDSSCs, the introduction of QDs offers new advantages of hot electron injection[5] and multi-exciton generation,[6] and the band gap of QDs can be adjusted by changing the particle size.[7] So far, a large variety of narrow band semiconductors, such as CdS, CdTe, CdSe, PbS, etc. have been used as the QD sensitizers in QDSSCs and the PCE has achieved more than 6%.[8-10]

Similar to the dye in conventional DSSCs, the QDs are excited by incident light to generate electron−hole pairs and the electrons are subsequently injected into TiO_2 conduction band, and then collected by the transparent conductive oxide electrode. At the same time, the holes are injected into the hole-transporting electrolyte and finally reach the counter electrode, on which the oxidized counterpart of the electrolyte is reduced. Therein, the morphology of photoanode plays a crucial role in the photovoltaic performance of QDSSCs and various TiO_2 photoanodes have been fabricated. For example, TiO_2 arrays composed of nanotube, nanowires, or nanorods as photoanode have been utilized in QDSSCs and significantly improved the PCE of the devices.[11-13] Recently, novel hierarchical TiO_2 structures have attracted considerable attention as promising photoanode materials.[14-16] Mesoporous anatase TiO_2 beads with high surface areas and controllable pore sizes prepared through a combined sol-gel and solvothermal process effectively promoted the PCE of corresponding DSSC device than P25-based DSSC.[17] Surfactant-directed self-assembly of size-tunable mesoporous TiO_2 microspheres was also employed in quasi-solid state DSSCs, which provided efficient light harvest and charge collection.[18] In addition, three dimensional hierarchical TiO_2 nanotube branches assembled onto the primary hollow TiO_2 nanofibrous backbone could offer large surface area for high QD loading and high light-scattering property.[19] The hierarchical TiO_2 microspheres consisting of nanorods and nanoparticles were also employed in QDSSCs and achieved a PCE over 4%.[20]

Hitherto, the influence of the hierarchical photoanode morphologies on the photovoltaic performance of QDSSCs is focused on the investigation of the factors such as particle structure, pore size distribution and light-harvesting effect, and so on.[14-19] In fact, the affect of morphologies on the trap states, charge transport and recombination kinetics of the device is also noteworthy. In general, the distribution of trap states could be obtained by measuring the chemical capacitance C_μ through electrochemical impedance spectroscopy.[21-23] By comparing the C_μ values of photoanode with and without loading QDs, Zaban *et al.* has confirmed that the QDs surface states may contribute to the experimental distribution of trap states.[21] And the surface states of photoanode materials are also found to exist in the photoelectrode and can be effectively eliminated by surface modification such as $TiCl_4$ treatment.[22, 23] Actually, the energy states referring to photoanodes of QDSSCs with different materials and morphologies need further study. In the traditional DSSCs, the trap states play a key role in the charge transport, which can be described by the multiple-trap model or the hopping model. The former model assumes that electrons in trap states have to be activated to the conduction band to participate in the charge transport, while the latter assumes a tunneling mechanism in the intra-gap states.[24-27] However, it is unclear if either of the models is applicable to the charge transport in QDSSCs. Besides, the recombination dynamic is also significantly influenced by the distribution of trap states. Bisquert *et al.* have proposed a typical recombination model in DSSCs with three distinct classes: (a) the conduction band states with a constant recombination rate; (b) the exponential distribution of bulk trap states obeying the multiple-trap limited recombination mechanism; (c) the iso-energetic surface states with a minimum parabolic velley.[28] So far, the recombination mechanisms and models in QDSSCs still lacks systematic study and Bisquert's model might be used for reference. In addition, the recombination dynamics in QDSSCs is usually measured by means of electrochemical impedance spectroscopy (EIS), intensity modulated photovoltage spectroscopy (IMVS) or open-circuit photovoltage decay, which has their own advantages of easy operation and analysis. [21-23, 29, 30] In contrast, another effective technique, the transient photovoltage (TPV) measurement, is time-consuming, but it is advantageous in providing the dynamic result at different energy states by modulating bias light intensities. [31]

Obviously, the study on the preparation of QDSSCs with hierarchical TiO2 microspheres has achieve a lot of progress, while the involved mechanism research seems insufficient, especially about the trap states distribution and charge transport/recombination dynamics. In this work, based on two kinds of QDSSCs with P25 and HMS as photoanode material respectively, the distribution of trap states and the charge transport dynamics is measured by the technique of time-resolved charge extraction (TRCE).[32, 33] In addition, the influence of trap states on the recombination dynamics is investigated by TPV measurement with different bias light intensities. Finally, a physical model involving trap states distribution, charge transport and recombination is put forth upon the related experimental results.

2. Experimental Section

2.1 HMS Preparation

The HMS particles were prepared according to our previous work.[34] Briefly, 0.65 g of P25 was dispersed in a mixture solution of 87.5 mL of hydrogen peroxide (H_2O_2, 30 wt %) and 12.5 mL of ammonia (NH_4OH, 26–28 wt %). The mixture was stirred for 24 h and converted to clear orange precursor solution. Afterwards, 20 mL of the precursor, 20 mL of distilled water and 40 mL of ethanol were transferred into a 100 mL Teflon container, which was then sealed tightly with a stainless jacket and heated at 160 °C for 30 min. After washing with water, the white precipitate was dispersed into the 40 mL distilled water and sealed in a 50 mL Teflon-lined autoclave and heated at 180 °C for 6 h. The final white precipitate was then washed with water and ethanol several times. The average size of as-prepared HMS is ~400 nm with specific surface area about ~ 100 $m^2 g^{-1}$ while the specific surface area of commercial P25 (Degussa) is about 50 $m^2 g^{-1}$.

2.2 QDSSC fabrication

The photoanode was prepared according to the literature. [35] Hydroxypropyl cellulose (Aldrich) was added into the polyethylene glycol with weight ratio of 10% and stirred at 100 °C for 6 h to yield the paste. Different TiO_2 materials (P25 or HMS) were added into the paste with vigorous stirring to prepare the uniform slurries, which was coated onto the substrate by doctor-blade method. After drying at room temperature, the photoanode was calcinated at 450 °C for 30

min with heating rate of 5 °C min^{-1}. The photoanode film was treated in 40 mM $TiCl_4$ solution in an oil bath at 70 °C for 30 min and then calcinated at 450 °C for 30 min with the same heating rate.

A modified chemical bath deposition method was applied for the deposition of the QDs on the TiO_2 photoanode.[36, 37] To load the CdS QDs, TiO_2 photoanode was immersed in an aqueous solution with the composition of 0.02 mM $CdCl_2$, 0.14 mM thiourea, 0.07 mM NH_4Cl and 0.23 mM ammonia with a final pH of ~9.0 in the chemical bath at 10 °C for 45 min. Afterwards, the CdSe QDs were deposited by immersing the films in an aqueous solution containing 0.026 mM $CdSO_4$, 0.04 mM $N(CH_2COONa)_3$ and 0.026 mM Na_2SeO_3 for 6 h in the same way. Finally, the films were treated with ZnS passivation by twice dipping alternatively into 0.1 M $Zn(CH_3COO)_2$ and 0.1 M Na_2S solutions for 1 min per dip, rinsing with deionized water between dips. The QD-sensitized photoelectrode and counter electrode were assembled to a sandwiched cell and the electrolyte composed of 1 M Na_2S and 1 M S in deionized water was injected into the slit *via* capillarity.

2.3 Photo-electrical measurements

TRCE is an established technique as reported in the previous work.[32, 33] The cell was illuminated from the substrate side by a Nd^{3+}: YAG laser (Quanta-Ray Pro-230 Series) with wavelength of 532 nm, pulse width of 10 ns, pulse energy of 170 μJ. The photovoltage signals were recorded by a digital storage oscilloscope (64Xs, Lecroy; Input impendence, 1 MΩ). At an indicated delay time during the photovoltage decay, a CMOS analog switch driven by a DG535 (Stanford Research System) was adopted to switch the cell from open circuit to short circuit. In this way, the charge stored in the cell can be extracted at the corresponding delay time (or photovoltage).

TPV is frequently used to evaluate charge recombination lifetime in the device. In order to study the relationship between the charge recombination rate and the open-circuit photovoltage, a green-light-emitting diode with central wavelength of 530 nm was used to generated different bias photovoltage (0-500 mV), and the transient photovoltage was recorded by the oscilloscope as mentioned above. A small perturbation photovoltage from 532 nm pulse laser was used to generate a small perturbation which is controlled less than 5% compared with the bias photovoltage.

3. Results and Discussion

<Fig. 1>

To investigate the influence of the HMS photoanode on the photovoltaic performance of QDSSCs, traditional P25 photoanode based QDSSC is also fabricated for reference. The photoanode morphology of the two types of devices is significantly different from each other, as shown in Fig. 1a and 1b. Obviously, P25 shows the morphology of random stacking from TiO_2 nanoparticle with the average size of ~25 nm. While HMS is microspheres with the diameter of ~400 nm, which are assembled from ~20 nm nanoparticles, as revealed in the inserted image of Figure 1b.[34] Due to the different photoanode materials, the two target devices demonstrate different photovoltaic performance. The *J-V* curves of the two devices are shown in Fig.1c, with the photovoltaic characteristics listed in Fig.1d. It can be seen that the PCE of Cell-HMS is 4.2%, which is 9% higher than that of Cell-P25 (3.8%). Besides, the two devices possess the same or similar open-circuit voltage (V_{oc}) and fill factor (FF). The increase of PCE in Cell-HMS should be owing to its higher short-circuit current density (J_{sc}) of 13.89 mA / cm^2 compared with 12.67 mA / cm^2 for Cell-P25.

According to the previous report, the significant increase of J_{sc} for microspheres photoanode is mainly attributed to the increase of photogenerated charges.[34] It is generally considered that microspheres with higher specific surface area can uptake more sensitizers and enhance the light scattering, promoting the absorption of incident light.[17, 18, 38] The incident photon-to-current conversion efficiency (IPCE) spectra demonstrated in Fig 1d can also confirm the superior light harvest effect for Cell-HMS compared with Cell-P25. Besides, the J_{sc} is determined by the efficiency of charge collection which is in turn controlled by photogenerated charge transport and recombination. Considering the importance of distribution of trap states to the charge transport and recombination, it is necessary to identify the relationship between the distribution of trap state, charge transport and recombination for the two devices.

3.1 Chemical capacitance and density of states

<Fig. 2>

TRCE is an effective technique to evaluate charge distribution and the dynamic of charge transport in the photoanode. As shown in Fig. 2, the black line represents the open-circuit photovoltage decay caused by recombination of the photogenerated electrons and the vertical colored lines are the extraction curves at indicated photovoltage (or

decay time) by switching the cell from open-circuit to short-circuit condition. The extracted charge (Q_{ex}) at different photovoltage (or decay time) can be obtained by integrating the extraction curves with decay time, as shown in Fig. 3a. It can be seen that the two cells show similar extracted charge at the region lower than 200mV. However, in the region higher than 200mV, the extracted charges for Cell-HMS increase more rapidly compared with that of Cell-P25, which may arise from the relatively higher density of trap states in Cell-HMS due to the grain boundaries among the assembled particles in microspheres or contacts between the microspheres and QDs.

<Fig. 3>

In addition, it is found that the extracted charge increases exponentially versus photovoltage, and the chemical capacitance C_μ can be calculated by taking the derivative with respect to Q_{ex}. Then the DOS of trap states can be obtained by DOS = $C_\mu/edS(1\text{-}p)$, where d is the films thickness, S is the effective area of photoanode, and p is the porosity.[39] The resulting chemical capacitance C_μ and DOS of the two types of devices are plotted in Fig. 3b. The C_μ values obtained for Cell-HMS are higher than Cell-P25, which is in consistent with the EIS result of TiO_2 microsphere-based QDSSCs.[40] Obviously, DOS increases exponentially versus photovoltage, and the trap states distribution can be fitted by the equation $C_\mu^{trap} = C_0^{trap}\exp(eV_{ph}/k_BT_0)$.[41-43] Then the characteristic energy k_BT_0 values can be calculated as 70 meV for Cell-HMS and 93 meV for Cell-P25, respectively, which indicates that Cell-HMS shows a shallower distribution of DOS and higher density of trap states. In another word, more electrons are distributed in the shallower trap states of Cell-HMS. Moreover, electrons with lower activation energy for Cell-HMS are prone to be extracted out and may effectively favor the charge collection even at lower photovoltage, which is in consistent with its relatively larger amount of extracted charge, as revealed in Fig. 3a.

3.2 Charge transport dynamics

<Fig. 4>

Apart from the distribution of trap states, TRCE can also give the information about charge transport dynamics.[33] Typical extraction kinetics consists of a fast photovoltage drop within 6μs and a subsequent slow decay, corresponding

to the discharge of substrate capacitance and chemical capacitance, respectively. The slow decay kinetics of the two devices is shown in Fig. 4, from which the charge transport in TiO_2 photoanode under short-circuit condition could be obtained. The photovoltage decay rate increase with the decrease of photovoltage for both devices and the apparent extraction time constant τ_{app} can be derived by exponential fitting to the decay curves, as is shown in Fig. 5a. Obviously, in the voltage region lower than 200 mV, the τ_{app} values of the Cell-HMS shows slightly larger than Cell-P25, while in the photovoltage region larger than 200 mV, the τ_{app} values of Cell-HMS increase much faster than Cell-P25, which may arise from the density of trap states as illustrated in Fig. 3a.

<Fig. 5>

However, it should be kept in mind that more electrons are populated at higher photovoltage and consequently a larger amount of charges should be extracted out in that case. Therefore, τ_{app} is an appropriate value determined by the amount of charges and the transport rate. In order to evaluate the comparable charge transport rate, the characteristic extraction time constant τ_c is defined by dividing τ_{app} with the corresponding extracted charges, implying the time constant for extracting out the same amount of charges. As shown in Fig. 5b, Cell-HMS demonstrates a slightly lower charge transport rate and the τ_c-V_{ph} curves can be fitted by exponential decay, which can be described as multiple-trap limited transport mechanism.[33] Although the average transport rate for Cell-HMS is calculated to be ~ 30 % lower with respect to Cell-P25, it should be noted that the average DOS increase for Cell-HMS is about five times larger than that of Cell-P25 in the region of 200 mV to 350 mV, as revealed in Fig. 3b. This indicates that the trapping and detrapping rate for Cell-HMS is much faster compared with Cell-P25. Meanwhile, the higher density of trap states in Cell-HMS means electrons must take more trapping and detrapping steps before they are eventually released to the conduction band within the multiple-trap frameworks, which would inevitably slow down the transport rate. On the other hand, electrons in Cell-HMS possess a lower characteristic energy, which are more likely to be activated and thus may accelerate the transport process. As a result, the higher density and shallower distribution of DOS, which influence the rate of charge transport from two opposite aspects, result in ~ 30 % lower transport rate for Cell-HMS compared with

Cell-P25. Obviously, in view of the transport process, such hierarchical structure would bring negative influence due to the high trap state density.

3.3 Charge recombination dynamics

<Fig. 6>

In addition to the charge transport kinetics, we have also investigated the recombination dynamics by means of TPV with different bias light intensities. Fig. 6a and 6b represent the normalized voltage curves of some characteristic transient photovoltage for Cell-P25 and Cell-HMS, respectively. It could be found that the relationship between the recombination rate and the photovoltage experiences three different procedures: (a) the recombination rate increases with photovoltage in the region of 0- 80 mV for Cell-P25 and 15-150 mV for Cell-HMS, respectively; (b) Along with the rise of photovoltage, the recombination rate turns to decreases in the region of 80-200 mV and 150-265 mV for Cell-P25 and Cell-HMS, respectively; (c) At even higher photovoltage, the recombination rate significantly increases with photovoltage. From the variation of recombination lifetime τ_n for different bias voltage illustrated in Fig. 6c, it can be seen that τ_n of Cell-P25 decreases in the photovoltage region of 0-80 mV, followed by an increase in the region of 80-200 mV, respectively. While for Cell-HMS, similar tendency is also observed with the evolution of τ_n appearing in the photovoltage region 15-150 mV and 150-265 mV, respectively. Beyond the maximum at 200 mV for Cell-P25 and 265 mV for Cell-HMS, the τ_n decreases continuously over photovoltage.

Obviously, the $\tau_n - V_{ph}$ plot involves two distinct regimes, a parabolic regime ($<$200 mV for Cell-P25 and $<$265 mV for Cell-HMS) and a linear regime at higher voltage region, which could be ascribed to different recombination mechanism. The charge recombination in the parabolic region is considered to be dominated by iso-energetic charge transfer through surface states, and the parabolic minimum represents the characteristic energy level of iso-energetic charge recombination, which is significantly influenced by the distribution of trap states.[28] The minimum of Cell-HMS is 80 mV and 150 mV for Cell-P25, indicating a 70 mV shift to high potential level for Cell-HMS, in consistent with its shallower DOS distribution. As the photovoltage increases beyond 200 mV and 265 mV for Cell-P25 and Cell-HMS

respectively, recombination lifetime decays exponentially as described by the multiple-trap limited recombination mechanism.[24, 28, 44] Besides, the intersection point for the two regimes is also closely related to the density of the trap states and is regarded as the boundary level dividing the lower-voltage iso-energetic charge recombination through surface states to higher-voltage multiple-trap limited recombination. The boundary voltage of 265 mV for Cell-HMS is 65 mV higher compared with 200 mV for Cell-P25, which is in consisted with its higher density of trap states. In addition, it could be noted that the average recombination rate for Cell-HMS is 96% lower compared with Cell-P25, which can be attributed to the higher surface area that could effectively load QDs and prevent the contact between TiO_2 and electrolyte.[37] Besides, the HMS photoanode with the large pores could allow the full electrolyte permeation and prolong the recombination lifetime.[18] The slower recombination rate for microsphere-based photoanode were also founded from the results of EIS in other reports.[45, 46] Therefore, although charge transport rate of Cell-HMS is about 30 % slower than that of Cell-P25, as mentioned above, the dramatic increase of the recombination lifetime leads to an efficient charge collection in Cell-HMS.

3.4 Influence of DOS on charge transport and recombination

<Fig. 7>

The aforementioned findings allowed us to propose a detailed scheme describing the influence of trap state distribution on charge transport/recombination, which is shown in Fig.7. With reference to Cell-P25, Cell-HMS shows higher overall trap state density but shallower DOS distribution, resulting in slower charge transport but faster trapping-detrapping processes. The charge recombination process is also significantly influenced by the trap states. The characteristic energy level of iso-energetic recombination through surface trap for Cell-HMS is 70 mV higher compared with that of Cell-P25, in accord with the shallower DOS distribution. Meanwhile, the boundary level from lower-voltage iso-energetic recombination to higher-voltage multiple-trap limited recombination also demonstrates a 65 mV upward shift for Cell-HMS with its higher density of trap states.

The dynamics performance would significantly affect photovoltaic parameters of the device. The much lower

recombination rate in Cell-HMS should benefit the increase of V_{OC}, [47-49] while the higher density of trap states would reduce the V_{OC} because more electrons are filled in the trap states. The two devices demonstrate a similar V_{OC} upon the influence of these opposite factors. Therefore, it can be concluded that trap states play a negative role in the device performance and should be reduced as far as possible. Actually, the trap states are expected to be distributed almost near the bottom edge of the conduction band. In this view, TiO_2 structure with enhanced crystal quality and less defects should be favorable as a photoanode materials for QDSSCs.

4. Conclusions

In summary, two kinds of QDSSCs with different photoanode morphology were prepared based on P25 and HMS photoanode to systematically study the DOS of the trap state, charge transport and recombination dynamics by means of TRCE and TPV techniques. Compared with Cell-P25, Cell-HMS shows a higher density of trap states and shallower distribution of DOS, which can influence the charge transport rate from two opposite ways within the multiple-trap limited transport mechanism. Cell-HMS shows a slightly lower transport rate but faster trapping and detrapping process compared with Cell-P25. In addition, the charge recombination rate for Cell-HMS is 96% lower than that of Cell-P25, which effectively promotes the charge collection. The characteristic energy level of iso-energetic charge recombination is 70 mV higher in Cell-HMS than that in Cell-P25 with different DOS distribution. Meanwhile, the boundary energy level dividing lower-voltage iso-energetic recombination and higher-voltage multiple-trap limited recombination is also found a 65 mV upward shift for Cell-HMS with the higher trap states density. Based on the experimental results, a detailed scheme is proposed to describe the effect of trap state distribution on charge transport/recombination. This work offers deeper insights into the operating mechanisms of QDSSCs, which can be helpful for further optimization of their photovoltaic performance.

Acknowledgements

The authors gratefully acknowledge the financial support from the Natural Science Foundation of China (Grant Nos. 21133001, 21173266 and 21473250) and the Fundamental Research Funds for the Central Universities, the Research Funds of Renmin University of China (Grant No. 11XNJ021).

References

1 A. Zaban, O. I. Micic, B. A. Gregg and A. J. Nozik, *Langmuir*, 1998, **14**, 3153.

2 P. V. Kamat, *J. Phys. Chem. C*, 2008, **112**, 18737

3 S. Rühle, M. Shalom and A. Zaban, *ChemPhysChem*, 2010, **11**, 2290.

4 S. Emin , S. P. Singh, L. Han, N. Satoh and A. Islam, *Solar Energy*, 2011, **85**, 1264.

5 W. A. Tisdale, K. J. Williams, B. A. Timp, D. J. Norris, E. S. Aydil and X.-Y. Zhu, *Science*, 2010, **328**, 1543.

6 J. B. Sambur, T. Novet and B. A. Parkinson, *Science*, 2010, **330**, 63.

7 G. Hodes, *J. Phys. Chem. C*, 2008, **112**, 17778.

8 N. Zhao, T. P. Osedach, L. - Y. Chang, S. M. Geyer, D. Wanger, M. T. Binda, A. C. Arango, M. G. Bawendi and V. Bulovic, *ACS Nano*, 2010, **4**, 3743.

9 P. Sheng, W. Li, J. Cai, X. Wang, X Tong, Q. Cai and C. A. Grimesb, *J. Mater. Chem. A*, 2013, **1**, 7806

10 J. Wang, I. Mora-Seró, Z. Pan, K. Zhao, H. Zhang, Y. Feng, G. Yang, X. Zhong and J. Bisquert, *J. Am. Chem. Soc.*, 2013, **135**, 15913.

11 W.-T. Sun, Y. Yu and H. - Y. Pan, *J. Am. Chem. Soc.*, 2008, **130**, 1124.

12 K. Žídek, K. Zheng, C. S. Ponseca, Jr., M. E. Messing, L. R. Wallenberg, P. Chábera, M. Abdellah, V. Sundstrom and T. Pullerits, *J. Am. Chem. Soc.*,2012, **134** , 12110.

13 J. Luo, L. Ma, T. He, C. F. Ng, S. Wang, H. Sun and H. J. Fan, *J. Phys. Chem. C*, 2012, **116**, 11956.

14 P. Yang, T. Deng, D. Zhao, P. Feng, D. Pine, B. F. Chmelka, G. M. Whitesides and G. D. Stucky, *Science*, 1998, **282**, 2244.

15 F. Zhu, D. Wu, Q. Li, H. Dong, J. Li, K. Jiang and D. Xu, *RSC Adv.* 2012, **2**, 11629.

16 P. B. Patil, S. S. Mali, V. V. Kondalkar, N. B. Pawar, K. V. Khot, C. K. Hong, P. S. Patilb and P. N. Bhosale，*RSC Adv.*, 2014, **4**, 47278.

17 D. Chen, F. Huang, Y. - B. Cheng and R. A. Caruso, *Adv. Mater.*, 2009, **21**, 2206.

18 W. Chen, Y. Qiu, K. Yan, S. Yang, *J. Power Sources*, 2011, **196**, 10806.

19 H. Han, P. Sudhagar, T. Song, Y. Jeon, I. Mora-Sero´, F. Fabregat-Santiago, J. Bisquert, Y. S. Kang and U. Paik, *Chem. Commun*., 2013, **49**, 2810.

20 X.-Y. Yu, J. -Y. Liao, K. - Q. Qiu, D. - B. Kuang, and C. - Y. Su, *ACS Nano*, 2011, **5**, 9494.

21 I. Hod, V. Gonzalez.-Pedro, Z. Tachan, F. Fabregat-Santiago, I. Mora-Seró, J. Bisquert and A. Zaban. *J. Phys. Chem. Lett.*, 2011, **2**, 3032.

22 Q. Huang, F. Li, Y. Gong, J. Luo, S. Yang, Y. Luo, D. Li, X. Bai and Q. Meng, *J. Phys. Chem. C*, 2013, **117**, 10965.

23 Q. Yu, Y. Wang, Z. Yi, N. Zu, J. Zhang, M. Zhang and P. Wang, *ACS Nano*, 2010, **4**, 6032

24 A. C. Fisher, L. M. Peter, E. A. Ponomarev, A. B. Walker and K. G. U. Wijayantha, *J. Phys. Chem. B*, 2000, **104**, 949.

25 L. M. Peter and K. G. U. Wijayantha, *Electrochem. Commun.*, 1999, **1**, 576.

26 J. Bisquert, *Phys. Chem. Chem. Phys.*, 2008, **10**, 3175.

27 J. Bisquert, *J. Phys. Chem. C*, 2007, **111**, 17163.

28 J. Bisquert, A. Zaban, M. Greenshtein and I. Mora-Seró, *J. Am. Chem. Soc.*, 2004, **126**, 13550.

29 K. Zhu, T. B. Vinzant, N. R. Neale and A. J. Frank, *Nano Lett*. 2007, **7**, 3739.

30 J. Bisquert, F. Fabregat-Santiago, I. Mora-Seró, G. Garcia-Belmonte and S. Gimenez, *J. Phys. Chem. C*, 2009, **113**, 17278.

31 L. Luo, C. - J. Lin, C. - S. Huang, C. - F. Lo, C. -Y. Lin and E. W. - G. Diau, *Phys. Chem. Chem. Phys.*, 2010, **12**, 12973.

32 N. W. Duffy, L. M. Peter, R. M. G. Rajapakse and K. G. U. Wijayantha, *J. Phys. Chem. B*, 2000, **104**, 8916.

33 Y. Wang, D. Wu, L. - M. Fu, X. - C. Ai, D. Xu and J. - P. Zhang, *Phys. Chem. Chem. Phys.*, 2014, **16**, 11626.

34 D. Wu, Y. Wang, H. Dong, F. Zhu, S. Gao, K. Jiang, L. Fu, J. Zhang and D. Xu, *Nanoscale*, 2013, **5**, 324.

35 F. Zhu, P. Zhang, X. Wu, L. Fu, J. Zhang and D. Xu, *ChemPhysChem*, 2012, **13**, 3731.

36 G. Hodes, *Phys. Chem. Chem. Phys.*, 2007, **9**, 2181.

37 D. Wu, X. Shi, H. Dong, F. Zhu, K. Jiang, D. Xu, X. Ai and J. Zhang, *J. Mater. Chem. A*, 2014, **2**, 16276.

38 G. Zhu, L. Pan, T. Xu and Z. Sun, *ACS Appl. Mater. Interfaces*, 2011, **3**, 1472.

39 B. C. O' Regan, K. Bakker, J. Kroeze, H. Smit, P. Sommeling and J. R. Durrant, *J. Phys. Chem. B*, 2006, **110**, 17155.

40 J. Yang, L. Pan, G. Zhu, X. Liu, H. Sun, Z. Sun, *J. Electroanal. Chem*, 2012, **677**, 101.

41 J. Bisquert, *Phys. Chem. Chem. Phys.*, 2003, **5**, 5360.

42 B. C. O' Regan, S. Scully and A. C. Mayer, *J. Phys. Chem. B*, 2005, **109**, 4616.

43 J. R. Jennings and Q. Wang, *J. Phys. Chem. C*, 2010, **114**, 1715.

44 J. Bisquert and V. S. Vikhrenko, *J. Phys. Chem. B*, 2004, **108**, 2313.

45 K. Fan, T. Peng, J. Chen, X. Zhang and R. Li, *J. Power Sources*, 2013, **222**, 38.

46 F. Xu, X. Zhang, Y. Wua, D. Wu, Z. Gao and K. Jiang, *J. Alloys Comp.* 2013, **574** , 227.

47 T. Marinado, K. Nonomura, J. Nissfolk, M. K. Karlsson, D. P. Hagberg, L. Sun, S. Mori and A. Hagfeldt, *Langmuir*, 2010, **26**, 2592.

48 R. Li, X. Lv, D. Shi, D. Zhou, Y. Cheng, G. Zhang and P. Wang, *J. Phys. Chem. C*, 2009, **113**, 7469.

49 D. Wu, J. He, S. Zhang, K. Cao, Z. Gao, F. Xu and K. Jiang, *J. Power Source*, doi:10.1016/j.jpowsour.2015.02.062.

Figure captions

Fig. 1 Typical SEM images of (a) P25 and (b) HMS (inset is the high-magnification image), respectively. (c) *J*-*V* curves and (d) IPCE spectra of the two kinds of QDSSCs. (e) Photovoltaic parameters of the two devices under 1 sun illumination (AM 1.5, 100 mW / cm^2).

Fig. 2 Charge extraction kinetics trace of the open-circuit photovoltage (V_{ph}) decay for (a)Cell-P25 and (b) Cell-HMS (black lines), and the kinetics at indicated time (colored vertical lines) recorded by fast switching the cell from open circuit to short circuit.

Fig. 3 (a) Extracted charge (Q_{ex}) versus photovoltage (V_{ph}) for the two devices. (b) Chemical capacitance (C_{μ}, left coordinate) and density of states (DOS, right coordinate) versus photovoltage (V_{ph}) for Cell-P25 (solid lines) and Cell-HMS (dashed lines).

Fig. 4 TRCE kinetics of the slow decay region with the extraction time set to zero for (a) Cell-P25and (b) Cell-HMS, respectively. The black arrows indicate the decrease of the photovoltage.

Fig. 5 (a) The apparent extraction time τ_{app} and (b) Characteristic extraction time at different photovoltage for Cell-P25 and Cell-HMS, respectively.

Fig. 6 Normalized photovoltage decay of TPV for (a) Cell-P25 and (b) Cell-HMS, respectively. (c) Electron lifetime versus photovoltage for the two devices. The solid lines at the region higher than 300 mV are the corresponding linear fitting lines.

Fig. 7 Physical model of TiO_2 photoanode for Cell-P25 (black line) and Cell-HMS (red line), and the solid points are the characteristic energy level for iso-energetic recombination. The hollow points are the boundary level from iso-energetic recombination region to the multiple-trap limited recombination region.

Fig. 1 (X.J. Shi *et al.*)

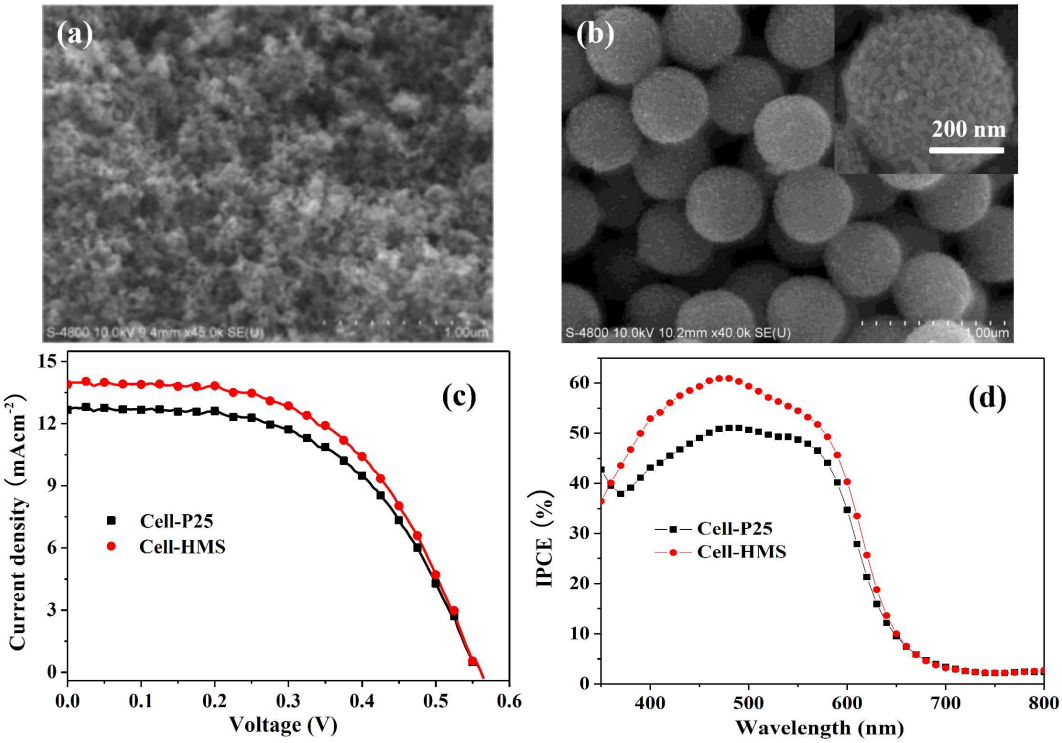

(e)

Samples	J_{SC} (mA/cm^2)	V_{OC} (mV)	FF	PCE (%)
Cell-P25	12.67	561	0.54	3.84
Cell-HMS	13.89	560	0.54	4.20

Fig. 2 (X.J. Shi *et al.*)

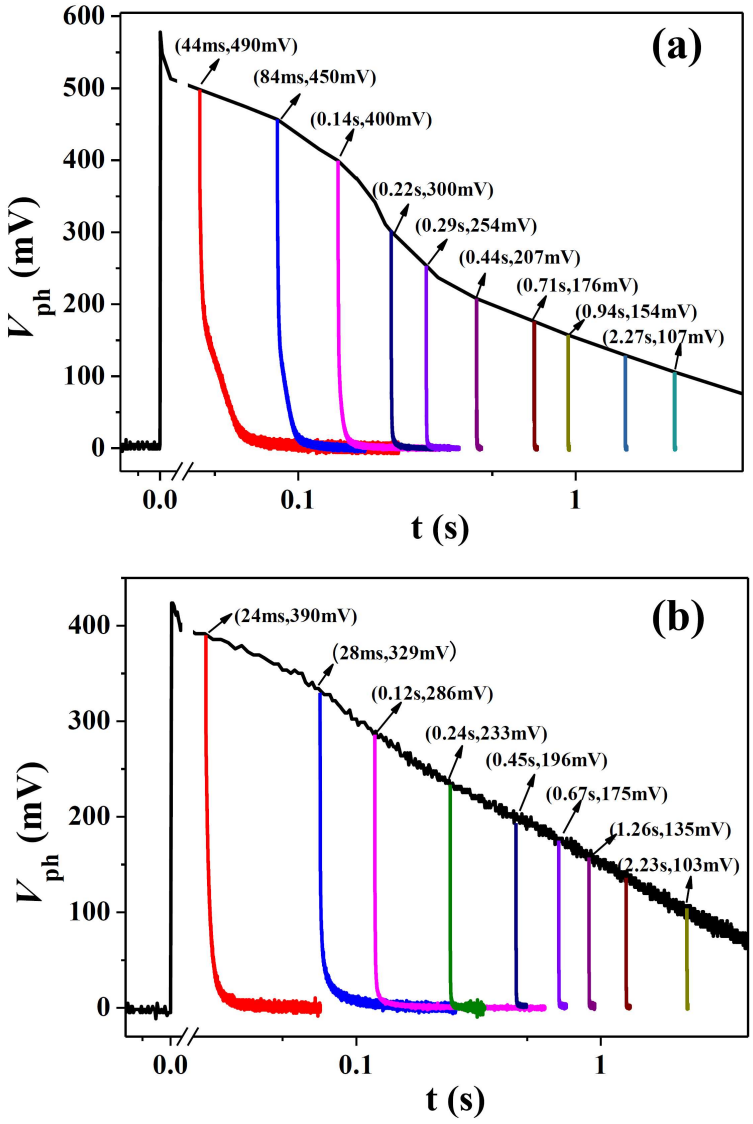

Fig. 3 (X.J. Shi *et al.*)

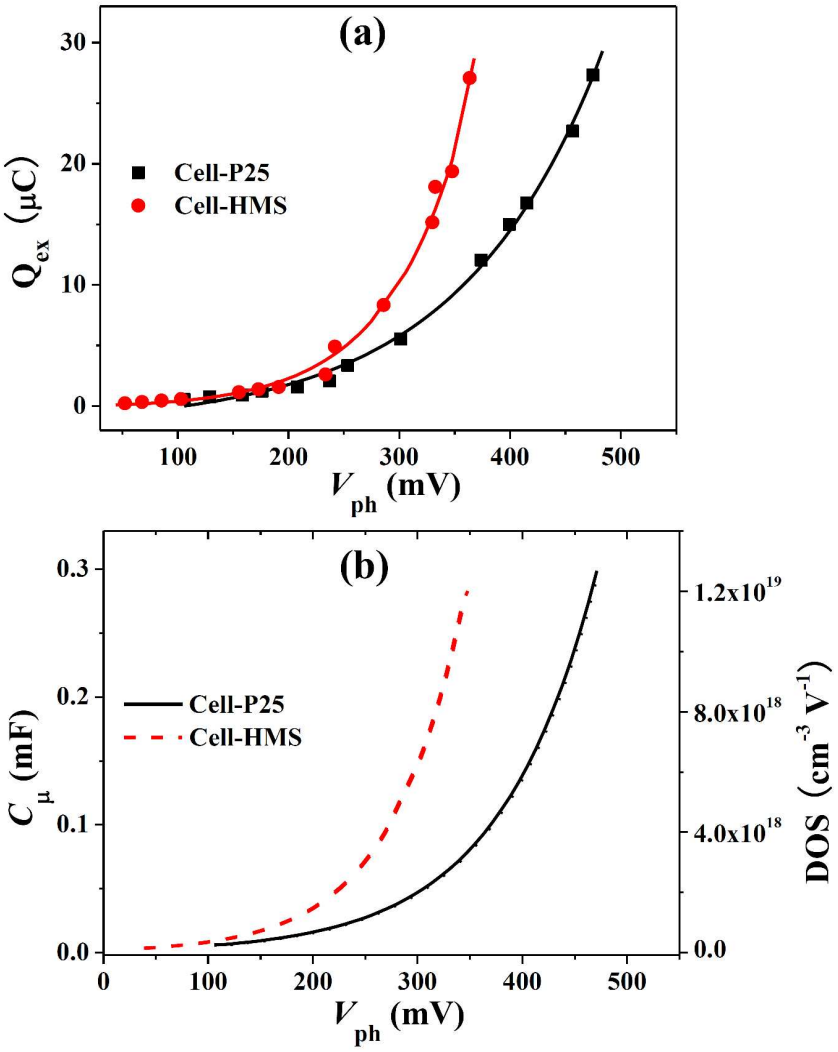

Fig. 4 (X.J. Shi *et al.*)

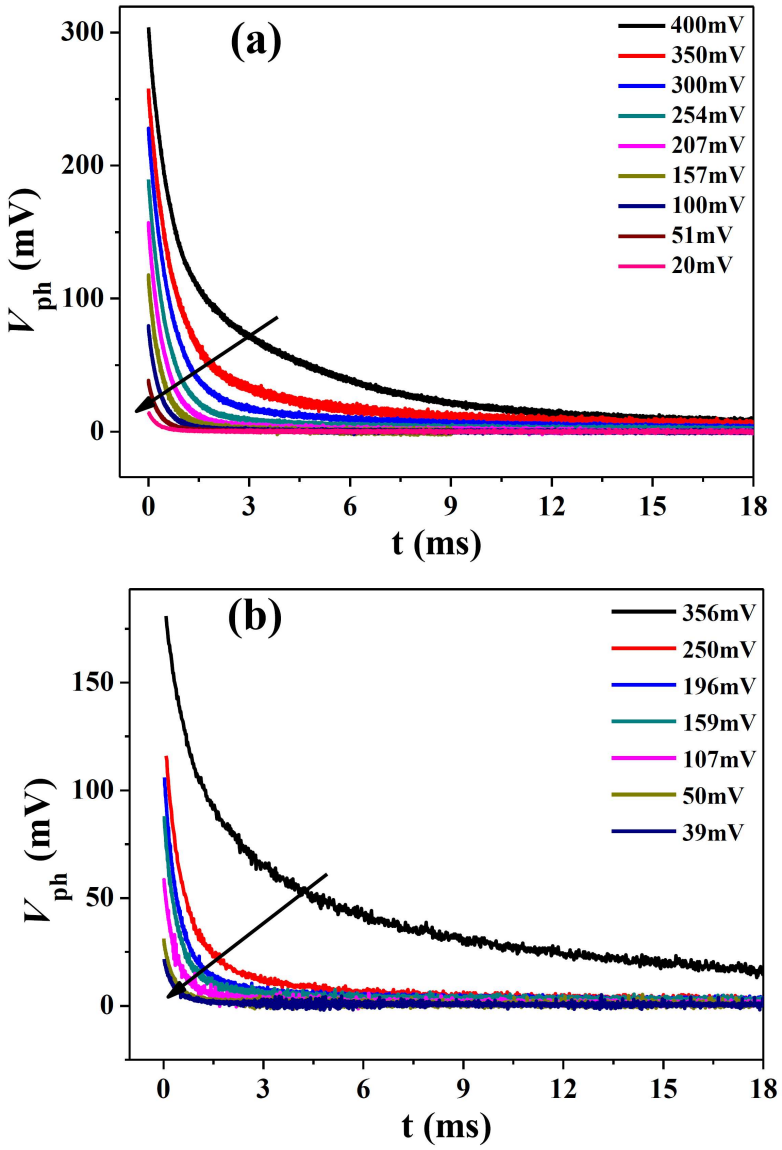

Fig. 5 (X.J. Shi *et al.*)

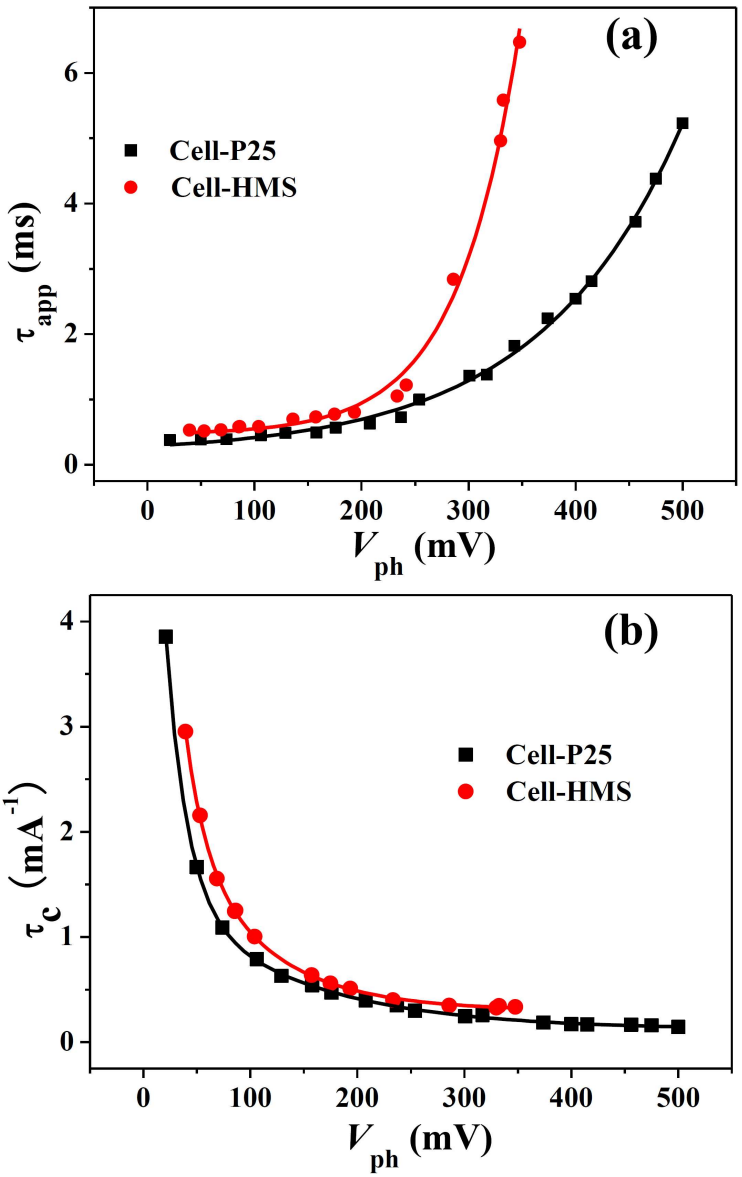

Fig. 6 (X.J. Shi *et al.*)

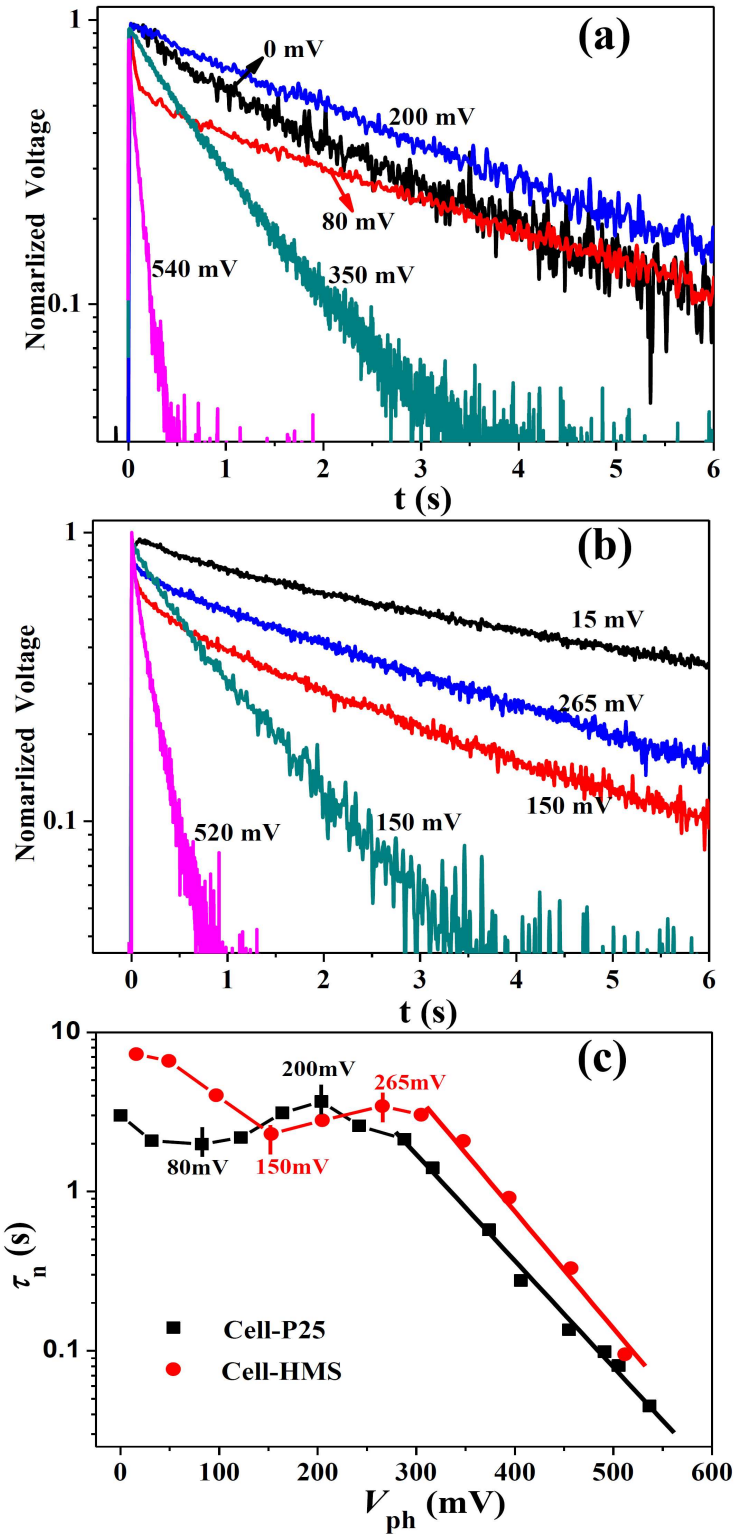

Fig. 7 (X.J. Shi *et al.*)

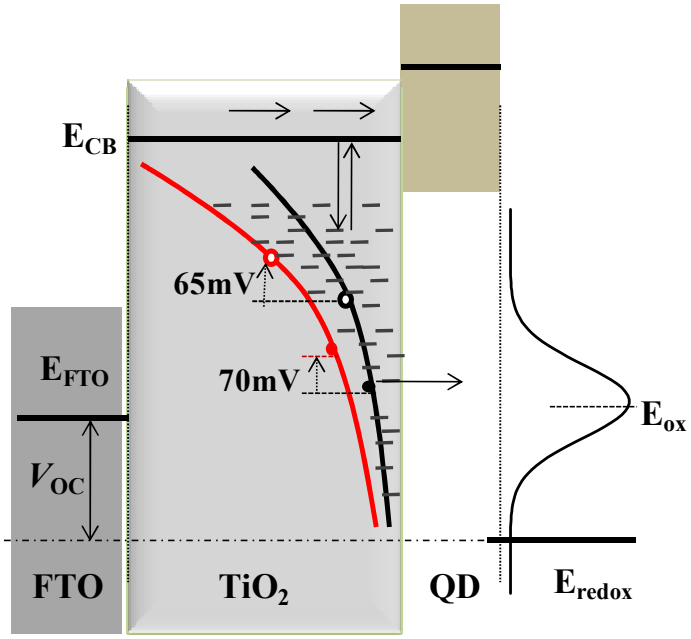

The table of contents entry

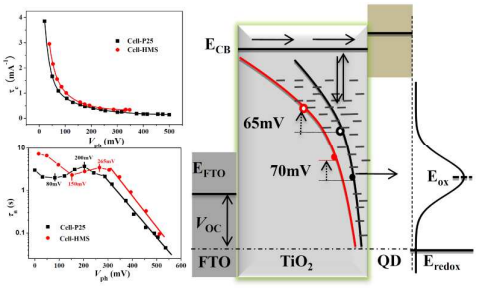

Highlight：The trap states distribution in the hierarchical TiO2 microspheres and their influence on charge transport/recombination dynamics